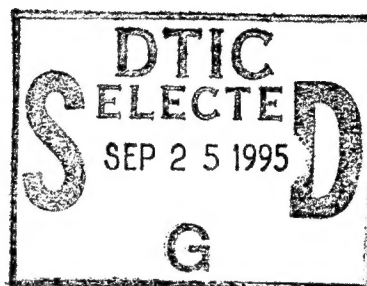RL-TR-95-97
Final Technical Report
May 1995

A RESEARCH REPORT ON VERTICAL-CAVITY SURFACE-EMITTING LASERS

University of Virginia

Elias Towe

DTIC
SELECTED
SEP 2 5 1995
G

APPROVED FOR PUBLIC RELEASE; DISTRIBUTION UNLIMITED.

19950919 207

Rome Laboratory
Air Force Materiel Command
Griffiss Air Force Base, New York

This report has been reviewed by the Rome Laboratory Public Affairs Office (PA) and is releasable to the National Technical Information Service (NTIS). At NTIS it will be releasable to the general public, including foreign nations.

RL-TR-95-97 has been reviewed and is approved for publication.

APPROVED: *Michael Turbyfill*

MICHAEL TURBYFILL, 1LT, USAF
Project Engineer

FOR THE COMMANDER: *Donald W. Hanson*

DONALD W. HANSON
Director of Surveillance & Photonics

REPORT DOCUMENTATION PAGE

Public reporting burden for this collection of information is estimated to average 1 hour per response, including the time for reviewing instructions, searching existing data sources, gathering and maintaining the data needed, and completing and reviewing the collection of information. Send comments regarding this burden estimate or any other aspect of this collection of information, including suggestions for reducing this burden, to Washington Headquarters Services, Directorate for Information Operations and Reports, 1215 Jefferson Davis Highway, Suite 1204, Arlington, VA 22202-4302, and to the Office of Management and Budget, Paperwork Reduction Project (0704-0188), Washington, DC 20503.

1. AGENCY USE ONLY (Leave Blank)	2. REPORT DATE May 1995	3. REPORT TYPE AND DATES COVERED FINAL Mar 93 – Aug 94

4. TITLE AND SUBTITLE
A RESEARCH REPORT ON VERTICAL-CAVITY SURFACE-EMITTING LASERS

6. AUTHOR(S)
Elias Towe

5. FUNDING NUMBERS
C - F30602-93-C-0010
PE - 62702F
PR - 4600
TA - P1
WU - PM

7. PERFORMING ORGANIZATION NAME(S) AND ADDRESS(ES)
University of Virginia
Thornton Hall
Charlottesville VA 22903-2442

8. PERFORMING ORGANIZATION REPORT NUMBER
N/A

9. SPONSORING/MONITORING AGENCY NAME(S) AND ADDRESS(ES)
Rome Laboratory/OCPC
25 Electronic PKY
Griffiss AFB NY 13441-4515

10. SPONSORING/MONITORING AGENCY REPORT NUMBER
RL-TR-95-97

11. SUPPLEMENTARY NOTES
Rome Laboratory Project Engineer: Michael Turbyfill, 1LT, USAF/OCPC/(315) 330-3147

12a. DISTRIBUTION/AVAILABILITY STATEMENT
Approved for Public Release; distribution unlimited.

12b. DISTRIBUTION CODE

13. ABSTRACT (Maximum 200 words)

The major accomplishments of this work were: (i) the growth, fabrication and testing of vertical-cavity surface-emitting lasers on (001) GaAs substrates---the device structures were grown by the technique of molecular beam epitaxy; (ii) the study of the polarization characteristics of these devices and (iii) the demonstration that there is no intrinsic polarization selection mechanism in surface-emitting lasers grown on (001) GaAs substrates. Because of the importance of the need for polarization stability of these devices for certain applications, a preliminary study to find techniques to control the polarization was carried out. During this work, it was demonstrated that it is possible to control the polarization of these devices when the substrate orientation is changed to the (110) direction. This preliminary study will be pursued in the next phase of our work. The work performed under this contract also resulted in six technical publications in professional journals. Furthermore, a total of four graduate students received advanced degrees with theses that were based on work supported by this contract. Two of the students were Air Force personnel at the Air Force Institute of Technology at WAFB and the other two were University of Virginia students.

14. SUBJECT TERMS
See Reverse

15. NUMBER OF PAGES
44

16. PRICE CODE

17. SECURITY CLASSIFICATION OF REPORT UNCLASSIFIED	18. SECURITY CLASSIFICATION OF THIS PAGE UNCLASSIFIED	19. SECURITY CLASSIFICATION OF ABSTRACT UNCLASSIFIED	20. LIMITATION OF ABSTRACT SAR

NSN 7540-01-280-5500

14. SUBJECT TERMS   (001) substrate, (110) substrate,
vertical-cavity surface-emitting laser (VCSEL), distributed
Bragg reflector (DBR), molecular beam epitaxy (MBE), polarization
control quantum well, GaAs, InGaAs, AlGaAs

Contents

Executive Summary

This report summarizes the work accomplished during the period running from March 1993 through June 1994 under contract No. F30602-93-C-0010. The major accomplishments of this work were: (i) the growth, fabrication and testing of vertical-cavity surface-emitting lasers on (001) substrates; (ii) the demonstration of a new technique for the control of the polarization of vertical-cavity surface-emitting lasers, and (iii) the publication of 6 papers in professional journals and conference proceedings reporting the technical details of the work performed during the contract period.

Accesion For		
NTIS CRA&I		☒
DTIC TAB		☐
Unannounced		☐
Justification		
By		
Distribution /		
Availability Codes		
Dist	Avail and / or Special	
A-1		

1. Introduction

Vertical-cavity surface-emitting lasers (VCSELs) have been a subject of intense research over the last few years because of some of their superior operating characteristics over conventional, edge-emitting semiconductor lasers [1, 2] The traditional semiconductor laser consists of a horizontal resonator terminated by mirrors at each end. The typical length of the resonator ranges from about 200 to 450 μm. Devices shorter and longer than these dimensions have also been made. Between the mirrors resides the active medium which also acts as an optical waveguide. The mirrors are typically formed by cleaving the resonator mechanically along a natural cleavage plane of the crystal out of which the laser is fabricated. The cleavage plane is usually orthogonal to the resonator axis. In cases where mechanical cleaving is not possible or desired, the resonator mirrors are formed by chemical etching. This type of device geometry complicates the fabrication process and it limits the integration potential of these lasers into multi-device optoelectronic circuits. The device geometry of the VCSEL, on the other hand, is ideal for integration with other optoelectronic devices. The VCSEL is usually constructed monolithically using either the crystal growth technique of molecular beam epitaxy or metal-organic chemical vapor deposition; in contrast to the edge-emitting device, the VCSEL has a vertical resonator with integral Bragg distributed reflector mirrors formed in one process sequence which includes the growth of the active region. From the substrate up, first, a Bragg reflector mirror is grown; then the active region is grown; and finally, the top Bragg distributed reflector mirror is grown. Individual devices can then be fabricated by standard lithographic techniques. The lithographic regions defining individual devices can be of any geometry—with circular apertures being the most common. Because the active volume under the aperture is geometrically uniform, surface-emitting lasers typically emit circular, low divergence beams. In edge-emitting lasers, the emitting aperture and hence the distribution of active material is typically rectangular. Because of the fundamental laws of diffraction, these edge-emitting laser apertures lead to elliptical, fan-shaped light beams which require imaging optics to correct the astigmatism before the light can be used in applications such as optical disc writing and laser printing.

A graphical illustration of the geometries of the two laser types is shown in Fig. 1.1. These geometries clearly reveal some of the obvious structural differences between the two devices from which a few of the technical advantages of the VCSEL can be inferred. The cavity length of a VCSEL, for example, is two orders of magnitude shorter than that of the

edge-emitting laser. One consequence of this is that the VCSEL typically lases in a single longitudinal mode compared to the multi-longitudinal mode emission of the edge-emitting device; another consequence is the smaller threshold current required for lasing in VCSEL devices. This is a result of the smaller active volume.

Vertical cleavage mirror
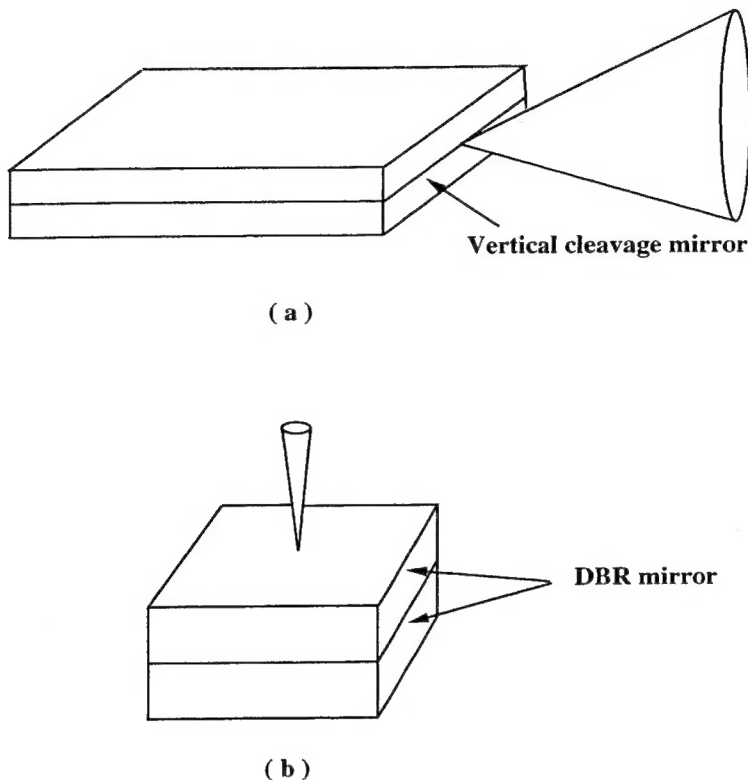
(a)

DBR mirror

(b)

Fig. 1.1: A schematic diagram of (a) an edge-emitting laser diode, and (b) a vertical-cavity surface-emitting laser diode.

Perhaps the single most important factor which has fueled the intensive research on the VCSEL has been the potential for large scale integration of two-dimensional arrays of this device with other optoelectronic devices [3, 4]. Since its invention in 1977 by Iga [1], an impressive catalogue of properties superior to the edge-emitting device have been demonstrated. The list of potential applications is also growing. Some of these applications include use in free-space optical interconnects, neural networks, laser printing, optical disc-recording, acousto-optic signal processing, and others yet to be thought of. Tremendous progress has been made in improving the basic operating characteristics of the VCSEL. Threshold currents have been reduced to values as low as microamperes [7]; optical power outputs have increased to several tens of milliwatts and quantum efficiencies of over 70%

have been demonstrated; VCSELs which operate in a continuous-wave mode with spectral outputs ranging from the visible to the near infrared have also been demonstrated [8].

One problem, however, still remains unsolved; this problem is the control of the polarization of the emitted light of VCSELs. The polarization of any coherent light source is an important basic property of the source. In coherent communications systems, for example, the polarization could carry additional information; in magneto-optic recording, the polarization of the source is an integral property of the system.

The light emitted by a typical VCSEL device fabricated from a structure grown on a (001) GaAs substrate is linearly polarized; the relative direction of the polarization, however, is random [9]. This behavior is a result of the isotropic gain in [001]-oriented active regions. The isotropic response of the feedback mechanism to all polarization eigenstates in the resonator also does little to set the relative polarization direction. For the most part, very little can be done to control the relative direction of polarization in devices fabricated on exact virgin (001) substrates. There is, however, evidence which suggests that a small anisotropy induced along any of the lateral crystallographic directions of the substrate can affect the relative state of polarization of a VCSEL [10]; this anisotropy can be introduced either during the growth of the structure or during device fabrication. The light emitted by VCSELs grown on (001) GaAs substrates is usually found to be polarized along two orthogonal directions; these directions, as implied earlier, are not fixed—but the most common mutually orthogonal directions usually observed are the [110] and the [$\bar{1}$10] crystallographic directions.

Several approaches have been proposed for the control of polarization states in VCSEL devices over the last few years. In 1991, Shimizu *et al.* [11] proposed a method in which high refractive index films are deposited on the side walls of a dielectric multilayer reflector to cause the reflectivity of the mirror to be anisotropic. They concluded that it was possible to control the polarization of a VCSEL by this method; so far, however, no experimental results have been reported because of experimental difficulties in realizing practical devices. Yet another technique which was proposed by Mukaihara *et al.* [12], involves the etching of an elliptical-shaped via in the device substrate into which a material with a larger thermal expansion coefficient is deposited; this leads to a gain with an anisotropic transverse distribution. The authors have reported polarization control with a success rate of about 80%. In 1993, Choquette *et al.* [13] reported a method that involves the use of novel transverse cavity structures with rhombus-like shapes. At low injection currents these devices operated with

5

the output polarization aligned along the longer axis of the rhombus. At higher injection currents, the output was observed to be polarized in two orthogonal directions; this meant that the polarization could not be stabilized by this technique. It appears that the methods which rely on gain anisotropy are the most promising. Another example of such a method has been reported by Chavez-Pirson *et al.*; in their approach, they use a fractional-layer superlattice in the gain medium to impart an anisotropic gain distribution [14]. A preliminary study has shown that there is polarization selectivity along the direction of maximum gain for optically pumped devices.

To date, most of the approaches reported add complexity to the fabrication process and would therefore increase the cost of the devices. Because of the importance of the polarization property of a VCSEL, a new approach for controlling the polarization is needed. Our approach has been to grow the VCSEL structure on non-(001) GaAs substrates where, in certain orientations, there is a natural symmetry-imposed anisotropy. To be specific, the (110) GaAs substrate has been chosen. Quantum well active regions grown on this surface exhibit optically anisotropic properties because the usual crystal symmetry which leads to isotropic quantum well properties on the (001) surface is broken on the (110) substrate.

The devices studied in this work have (In,Ga)As/(Al,Ga)As quantum wells in the active region and (Al,Ga)As/GaAs quarter wavelength stacks which act as distributed Bragg reflector (DBR) mirrors. The oscillation wavelength of the device was designed to be in the range of 900 to 1000 nm so that the light could be emitted through the (GaAs) substrate, if desired, since the substrate is transparent at these wavelengths. The monolithic device structure is grown by the method of molecular beam epitaxy. Index-guided VCSEL devices are fabricated using standard lithographic techniques which include wet and dry chemical etching.

Since the atomic surface structure of the (110) GaAs substrate is different from that of the conventional (001) substrate, the ideal growth conditions for the structures in this study must be determined; the problem of the control of doping incorporation must also be addressed. The growth of the device structures is, therefore, a central issue of this work.

This report will be organized as follows: In section 2, the principles of VCSEL design will be presented. The critical issues of Fabry-Perot cavity length, DBR design, loss and gain accounting and its relationship to the threshold current will be discussed. Section 3

will discuss the bulk of the experimental work necessary for the fabrication of the VCSELs. The growth of the structures by molecular beam epitaxy including the determination and stabilization of the growth rate will be discussed in this section. In section 4, we present some experimental results of VCSEL devices grown on (001) substrates. These devices exhibit the classic polarization randomness problem mentioned earlier. Finally, we present preliminary results of some VCSEL devices grown on (110) substrates. The polarization states of these devices are stable and well-controlled. We believe the growth of VCSEL structures on non-(001) substrates, such as the (110) used in our case study, offers a better approach to solving the polarization stability problem.

2. Design Considerations for Vertical-Cavity Surface-Emitting Lasers

2.1. Cavity Design

The basic structure of a vertical-cavity surface-emitting laser consists of a gain region sandwiched between two high reflectivity DBR mirrors. The entire structure is monolithically grown and it forms the Fabry-Perot cavity. In this study, the gain region is composed of several layers of (In,Al,Ga)As material designed to give a lasing wavelength which can range from about 900 nm to 1000 nm. The high reflectivity mirrors on either side of the active region are made of either AlAs/GaAs or (Al,Ga)As/GaAs layers. These mirrors provide the necessary optical feedback for the photons emitted from the recombination of the electron-hole pairs in the active region. When the optical gain exceeds the losses, lasing action is established and a coherent light beam is then emitted from the mirrors. A schematic representation of a typical vertical-cavity surface-emitting laser is shown Fig. 2.1. As the optical wave oscillates inside the cavity, a standing wave is established with a maximum field amplitude at the central gain region; this field amplitude decays at the mirror regions. For optimal performance, the total length of the gain region should be an integer multiple of the oscillation wavelength of the laser. To illustrate the principle, let us take this length to be equal to one full wave of the emission wavelength. The gain medium of the device can be a bulk material or a quantum well structure. In general, quantum well structures constitute better gain media than bulk materials. This is simply because (i) quantum wells occupy a smaller fraction of the Fabry-Perot cavity than bulk media and also the gain from quantum well structures is better matched to overlap the field intensity profile at the maximum location; (ii) the density of states for quantum well structures is smaller than that of bulk media, which means lower injection currents are required to achieve transparency, and (iii) the peak gain of quantum well structures is higher compared to that of bulk media of the same material for equivalent injection currents [15].

The energy-space band diagram of a typical active region for a vertical-cavity surface-emitting laser is illustrated in Fig. 2.2. This structure consists of a single (In,Ga)As quantum well surrounded by GaAs and (Al,Ga)As confining layers. The GaAs and (Al,Ga)As layers form a structure which simultaneously confines carriers and photons into this region. The
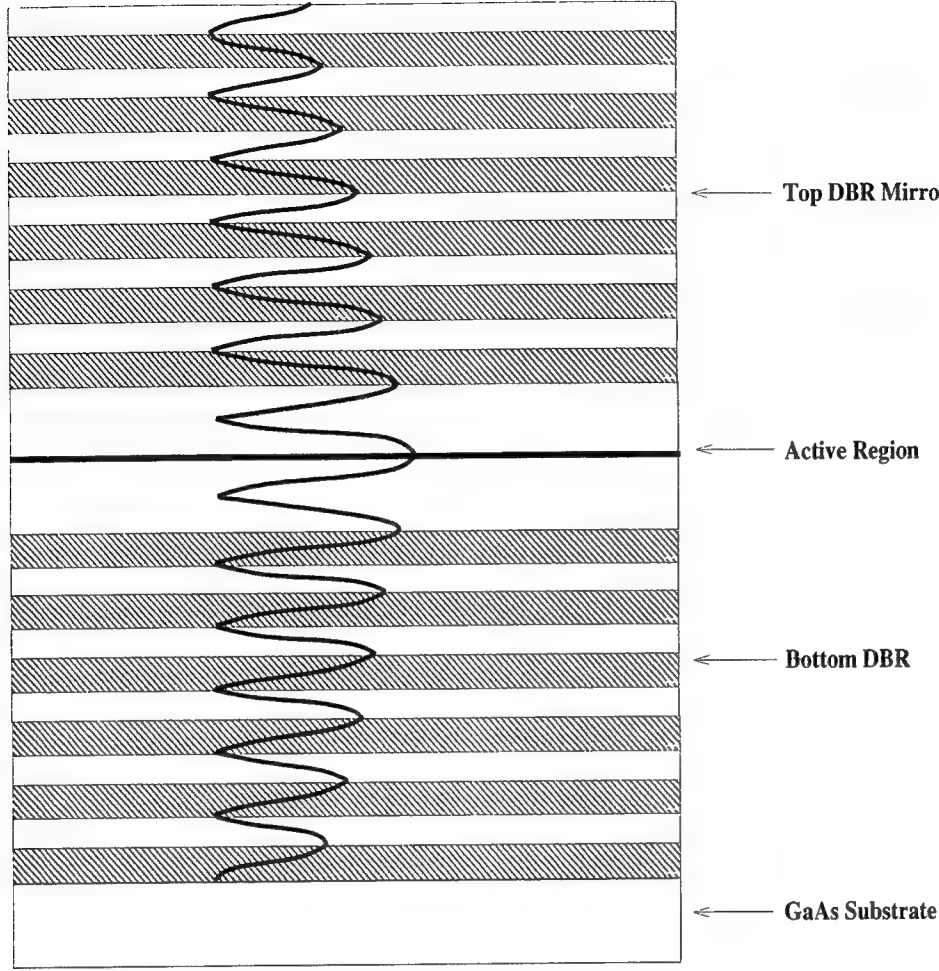
Fig. 2.1 A schematic diagram of a typical vertical-cavity surface-emitting laser with the field intensity distribution that forms a standing wave.

optimal length of the active region is designed to be an integer multiple of the operating wavelength. The thickness of each layer must therefore be determined from the relationship

$$2d_{AlGaAs}\, n_{AlGaAs} + 2d_{GaAs} n_{GaAs} + N d^w_{InGaAs} n^w_{InGaAs} + (N-1) d^b_{GaAs} n^b_{GaAs} = \lambda_0 \qquad (1)$$

where the $n_{i's}$ are the refractive indices of the respective layers of the materials in the active region, λ_0 is the lasing wavelength in vacuum, N is the total number of quantum wells, d^w_{InGaAs} is the width of a quantum well and d^b_{GaAs} is the thickness of a GaAs barrier. The lasing wavelength is generally close to the fundamental transition wavelength of the quantum well; that is, the $e \rightarrow hh1$ transition. This transition must be calculated by finding the eigen-energies of the quantum wells. The calculation begins by considering the Luttinger-Kohn formulation of the valence band Hamiltonian [16]. Since the (In,Ga)As quantum wells
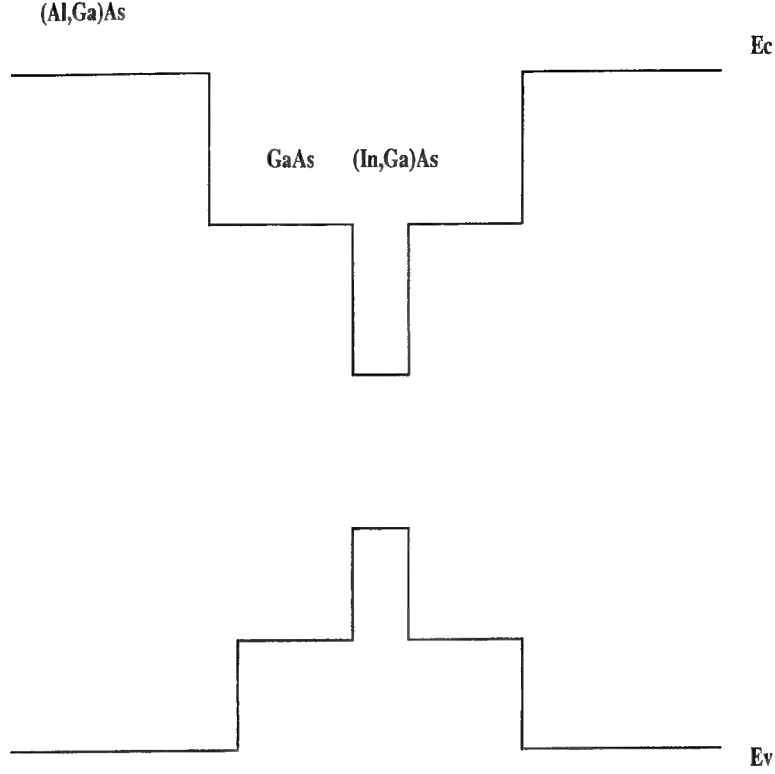
9

Fig. 2.2: The energy band diagram of the active region of a vertical-cavity surface-emitting laser.

used in this study are compressively strained, the change of bandgap induced by the strain must also be taken into account through the strain Hamiltonian or the so-called Bir-Pikus Hamiltonian. The details of this calculation will not be given here since we have already presented them elsewhere. The next important aspect of vertical-cavity surface-emitting laser design is the determination of the number of quarter wave stacks required for the distributed Bragg reflector mirrors. The design details of the mirrors are presented in the next section.

2.2. Distributed Bragg Reflector Mirror Design

The active region of a vertical-cavity surface-emitting laser is extremely short; typically, it is on the order of tens of nanometers thick. It can be shown quantitatively that for such short active regions, very high reflectivity mirrors are required in order for there to be sufficient feedback to support laser action at reasonable threshold currents. The required

mirror reflectivities are about 98%. There are several schemes to achieve reflectivities of this order; these schemes include the use of metallic mirrors such as gold; the use of dielectric quarter wave stacks to form distributed Bragg reflectors, or the use of quarter wave stacks composed of semiconductor materials. For this work, the use of semiconductor quarter wave stacks was the preferred scheme. This is simply because the formation of these mirrors can be accomplished in a single step process together with the growth of the active region; in other words, the whole device structure can be grown monolithically by the method of molecular beam epitaxy.

Our choice of the semiconductor materials to be used in the quarter wave stack consists of AlAs and GaAs layers. These materials have large relative bandgaps compared to the transition energy of the fundamental laser emission (900 to 1000 nm); this implies minimum absorption of the laser emission in these layers. Furthermore, GaAs and AlAs have about the same lattice constants so their epitaxial growth, one on top of the other, presents no major problems. The index differences between the two alloys is also relatively large, so high reflectivity structures with relatively few number of quarter wave stacks can be achieved. The typical mirror structure composed of GaAs (high index) and AlAs (low index) alternating quarter wave layers is shown in Fig. 2.3. The reflectivity of this distributed Bragg structure can be calculated by the characteristic matrix method [17]. A model which accounts for the field distribution in the mirrors can be used to calculate the effective reflectivity. According to this model, we assume that in each layer there are two counter-propagating electric field amplitudes. One field amplitude, E_i^+, travels in one direction and the other amplitude, E_i^-, travels in the opposite direction. Using the characteristic matrix method, one can relate E_0^+ and E_0^- in layer 0—which is the spacer layer—to E_1^+ and E_1^- in the low index layer 1 by the equation

$$\begin{pmatrix} E_0^+ \\ E_0^- \end{pmatrix} = \frac{1}{t_0} \begin{pmatrix} e^{i\delta_1} & r_0 e^{-i\delta_1} \\ r_0 e^{i\delta_1} & e^{-i\delta_1} \end{pmatrix} \begin{pmatrix} E_1^+ \\ E_1^- \end{pmatrix} \tag{2}$$

where

$$r_0 = \frac{n_l - n_0}{n_l + n_0} \tag{3}$$

and

$$t_0 = \frac{2n_0}{n_0 + n_l}; \tag{4}$$

for normal incidence; $\delta_1 = 2\pi n_l d_l / \lambda_0$; n_0 and n_l are, respectively, the indices of refraction of the spacer layer and the (low index) AlAs layer, d_l is the thickness of AlAs quarter wave layer. In similar fashion, we can express E_1^+ and E_1^- in terms of E_2^+ and E_2^- through use of
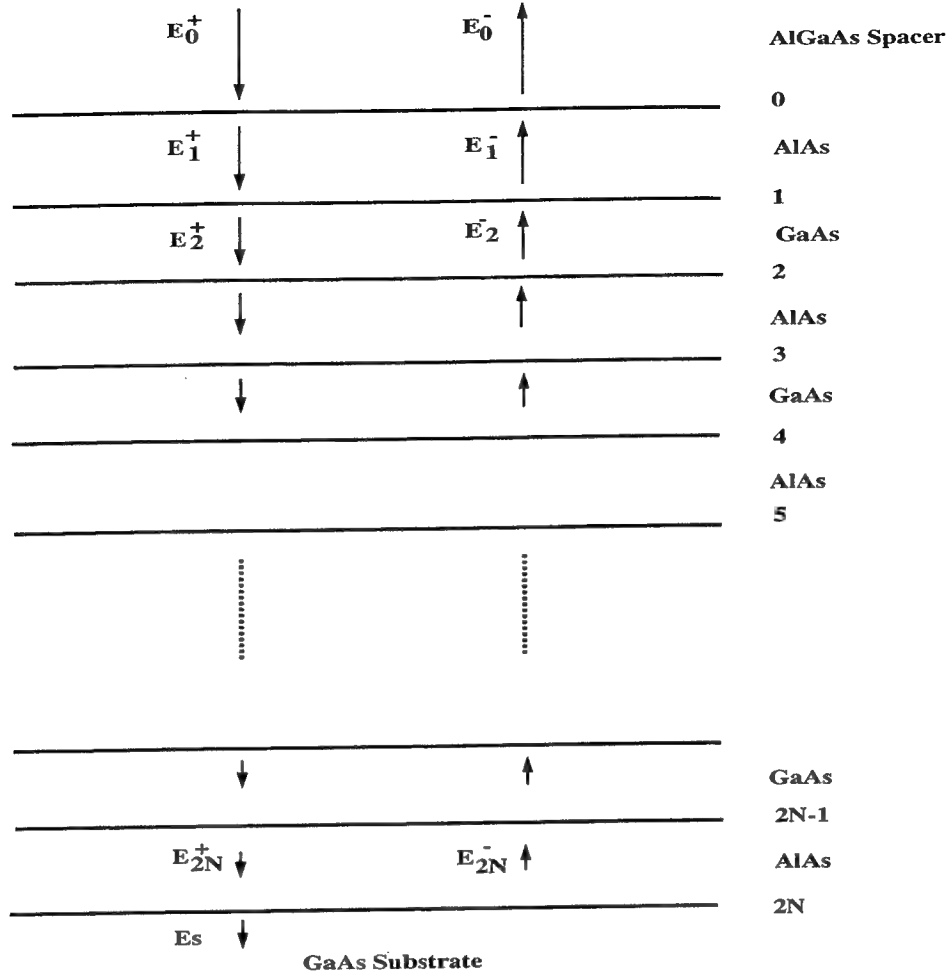
11

Fig. 2.3. A Schematic representation of a quarter wave GaAs/AlAs distributed Bragg reflector (DBR)

the following characteristic matrix:

$$\begin{pmatrix} E_1^+ \\ E_1^- \end{pmatrix} = \frac{1}{t_1} \begin{pmatrix} e^{i\delta_2} & r_1 e^{-i\delta_2} \\ r_1 e^{i\delta_2} & e^{-i\delta_2} \end{pmatrix} \begin{pmatrix} E_2^+ \\ E_2^- \end{pmatrix} \qquad (5)$$

where

$$r_1 = \frac{n_h - n_l}{n_l + n_h} \qquad (6)$$

and

$$t_1 = \frac{2n_l}{n_h + nl}; \qquad (7)$$

$\delta_2 = 2\pi n_h d_h / \lambda_0$; d_h and n_h are, respectively, the thickness and index of refraction of the GaAs quarter wave layer. Continuing this analysis for the other layers allows us to relate the electric fields E_{2N}^+ and E_{2N}^- in the other layers to the field E_s in the substrate. The field

E_s is a transmitted field without a reflected counterpart. The product of these characteristic matrices relate the initial field to the field in the substrate thus:

$$\begin{pmatrix} E_0^+ \\ E_0^- \end{pmatrix} = \frac{M_0 M_1 .. M_{2N-1}}{t_0 t_1 .. t_{2N-1} t_s} \begin{pmatrix} 1 & r_s \\ r_s & 1 \end{pmatrix} \begin{pmatrix} E_s^+ \\ 0 \end{pmatrix} \tag{8}$$

where the $M_{i's}$ are matrices of the form given above, $r_s = r_1$ and $t_s = t_1$. This equation can be simply written as

$$\begin{pmatrix} E_0^+ \\ E_0^- \end{pmatrix} = \begin{pmatrix} a_{11} & a_{12} \\ a_{21} & a_{22} \end{pmatrix} \begin{pmatrix} E_s^+ \\ 0 \end{pmatrix} \tag{9}$$

where the matrix elements, a_{ij}, are a result of multiplying the matrices M_i above. The reflectivity can then be extracted from the previous equation as

$$R = \left| \frac{E_0^-}{E_0^+} \right|^2 = \left| \frac{a_{21}}{a_{11}} \right|^2. \tag{10}$$

The numerical value of the reflectivity depends on the actual indices of refraction used. For the $Al_x Ga_{1-x} As$ materials system used here, the index is related to bandgap through the following empirical equation [18]:

$$n^2 = 1 + \frac{E_0 E_d}{E_0^2 - E^2} \tag{11}$$

with

$$E_0 = 3.65 + 0.871x + 0.179x^2, \tag{12}$$

$$E_d = 36.1 - 2.45x, \tag{13}$$

and

$$E = \frac{hc}{\lambda}. \tag{14}$$

The indices of refraction for the AlAs and GaAs alloys are $n_l(AlAs)=2.95$, $n_s(GaAs)=n_h = 3.52$ for $\lambda_0=0.98$ μm. The index difference for these alloys is $\Delta n = 0.57$. Substituting these numbers into the numerical equations used in the computations, one finds that about 20 pairs of quarter wave GaAs and AlAs stacks are necessary to achieve a peak reflectivity of about 99%. The calculated reflectivity spectrum of a DBR structure with 24 pairs of GaAs/AlAs quarter wave layers is shown in Fig. 2.4 for a center wavelength of 980 nm. Note that the spectrum has a flat region centered around 980 nm with a reflectivity of about 99.9%. This region is called the stop-band. Outside of the stop-band, the refelctivity drops and oscillates.
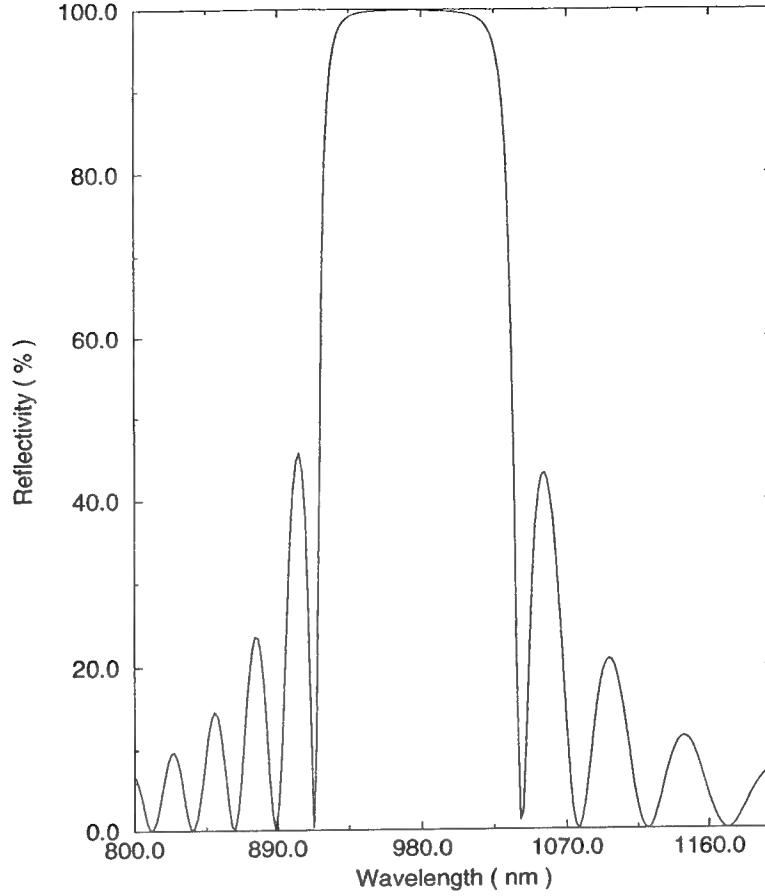
13

Fig. 2.4 A numerically calculated reflectivity spectrum of a quarter wave GaAs/AlAs DBR mirror.

The DBR mirror discussed above is for the bottom side of the VCSEL device, *i.e.*, the GaAs substrate side of the device. The top mirror is usually terminated by a p-type GaAs layer covered by an ohmic metal contact. This metal layer can increase the reflectivity of the top DBR mirror if the phase shift induced at the interface of the metal and the GaAs layer is matched such that the reflected electric field is in-phase with the upward traveling electric field. To increase the reflectivity, a gold layer is normally used for the p-type contact. The phase-shift and the reflection coefficient of a gold film on top of a GaAs layer is given by [19]

$$\phi = tan^{-1}\left(\frac{2n_h k_1}{n_1^2 - n_h^2 + k_1^1}\right) \tag{15}$$

and

$$R = \frac{(n_h - n_1)^2 + k_1^2}{(n_h + n_1)^2 + k_1^1} \tag{16}$$

where n_1 and k_1 are the real and imaginary parts of the index of refraction for gold. At the wavelength of 980 nm, $n_1 = 0.177$ and $k_1 = 5.973$. Thus, $\phi = 60°$ and the field reflectivity is $R = 0.974$. So the thickness of the GaAs phase-matching layer added on top of the quarter

14

wave GaAs can be determined from

$$2d\,n_h\,\frac{2\pi}{\lambda} = \pi - \frac{\pi}{3} \tag{17}$$

and at the peak wavelength of $\lambda_0 = 980$ nm, this thickness is about $d = 0.16\lambda_0$.

3. Electrical Properties of Distributed Bragg Reflector Mirrors

In a vertical-cavity surface-emitting laser, the electronic carriers share the same path with the photons in the DBR mirror regions. Although the semiconductor DBR mirror structure can provide high optical reflectivity, the accompanying energy band discontinuities at the hetero-interfaces results into barriers which carriers must surmount. These potential barriers impede carrier flow in the DBR structures and result in large series resistances. The problem is particularly severe for the holes in the valence band of the p-type DBR mirror. The series resistance gives rise to ohmic heating which causes deterioration of laser performance, especially in continuous-wave operation. Figure 3.1(a) shows the energy band diagram of a section of an undoped GaAs/AlAs quarter wave DBR. With p-type dopants, the band diagram will deform into the shape shown in Fig. 3.1(b). Potential spikes are formed at the hetero-interfaces due to space charge. The barrier height is roughly the valence band offset, $\triangle E_v$, between the GaAs and AlAs alloy. For a p-type GaAs/AlAs DBR, $\triangle E_v$ is about 250-300 meV which is much larger than the thermal energy at 300 K of 26 meV. The width of the barriers depends inversely on the square root of the doping level and is about 100 Å for several times of 10^{18}cm^{-3} doping concentration. Electric current conduction is either by thermionic emission for those holes with distribution energies exceeding the barriers or by quantum mechanical tunneling through the barriers for the others. The functional dependency of the thermionic current, I_{th}, on the barrier height is

$$I_{th} = I_1 \exp(-\triangle E_v/kT), \tag{18}$$

and that of the tunneling current I_{tn} is [20]

$$I_{tn} = I_2 \exp(-\beta \triangle E_v), \qquad \beta = (1/\hbar q)\sqrt{4m_h\epsilon/N_A} \tag{19}$$

where I_1 and I_2 are constants of proportionality, m_h is the hole effective mass, N_A is the acceptor concentration assuming full depletion, ϵ is the dielectric permittivity, and kT is
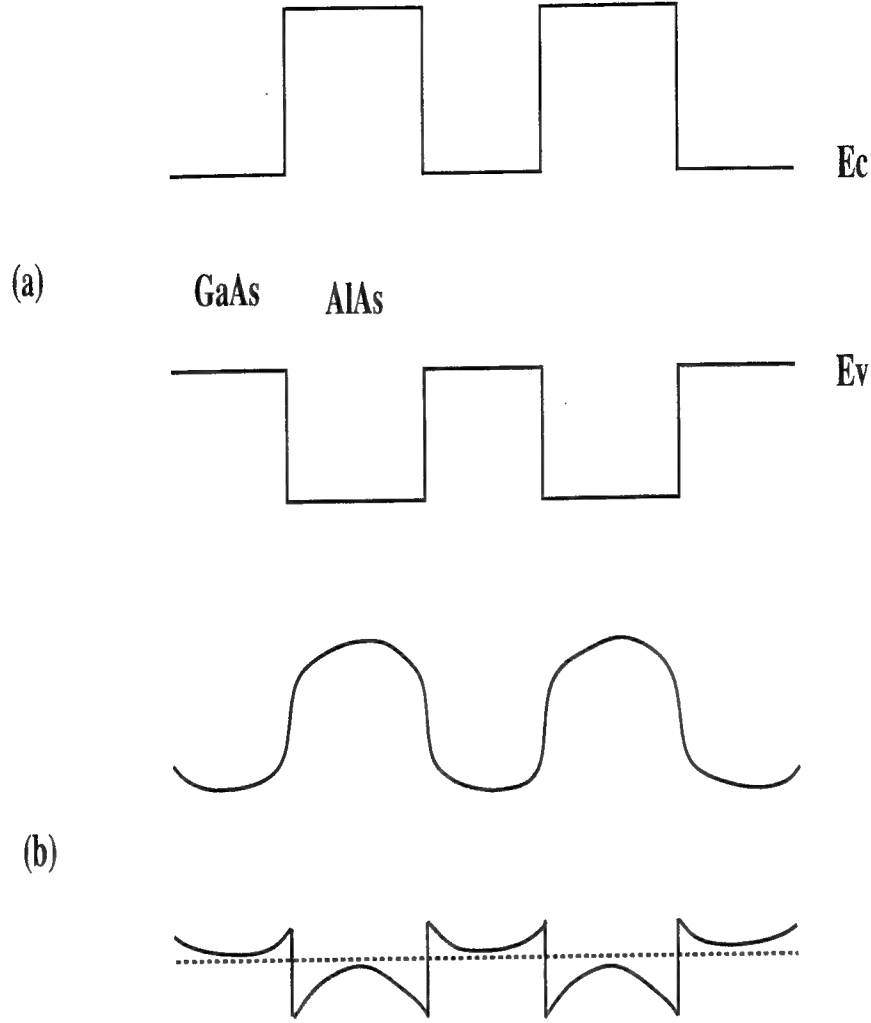
Fig. 3.1: The Energy band diagram of (a) an undoped GaAs/AlAs quarter wave DBR structure and (b) a p-type doped structure.

the thermal energy. As can be seen from these equations, reducing the potential barrier height and increasing the acceptor concentration at the hetero-interfaces, I_{th} and I_{tn} can be increased, *i.e.*, the series resistance of the p-doped DBR mirror can be decreased. The most obvious and simplest way to solve the high series resistance problem is to heavily dope the p-type DBR mirror; this, however, leads to greater optical loss because of free carrier absorption. Since the photons share the same path with the charge carriers, some of the photons will be absorbed by the free carriers. The carriers which absorb the photons are excited into higher energy states and return to the lower energy states through non-radiative pathways. In short, free carrier absorption generates heat and increases the threshold current of VCSELs.

Figure 3.2 shows several alternative approaches to reducing the series resistance. The first approach uses a graded $Al_xGa_{1-x}As$ layer with x varying from 0 to 1 between GaAs and AlAs layers (see Fig. 3.2(a)). The second approach uses an intermediate $Al_xGa_{1-x}As$ step-layer with $x = 0.5$ (Fig. 3.2(b)). These two techniques can reduce the effective potential barrier height and thus increase the thermionic current. The third approach uses a GaAs/AlAs superlattice (SL) structure between the GaAs and AlAs layers. The SL structure reduces the potential barrier height and simultaneously break the thick barrier into multiple thinner spikes which enhance the probability of quantum mechanical tunneling for the carriers. Any one of these approaches can reduce the series resistance of a p-type DBR mirror by a factor of about 100. When combined with increased doping density at the hetero-interfaces, the effective series resistance can be further reduced [21]. It should be pointed out that when the interface layers are added to the DBR stacks, the total optical thickness of a DBR pair, *i.e.*, the thickness of the high and low index layers plus the interface layers, should still be made equal to one half of the design lasing wavelength.

4.   Threshold Current Density and Quantum Efficiency

In this section, we analyze the relation between the threshold gain and the cavity loss in a VCSEL. The threshold current density depends on the gain required to reach transparency. The generic expression for the material gain required at the threshold is given as [8]

$$g_{th} = \frac{1}{\Gamma}\left(\alpha_i + \frac{1}{L}\ell n\frac{1}{R}\right) \tag{20}$$

where R is the mean reflectivity of the DBR mirrors, that is, $R = \sqrt{R_t R_b}$, R_t and R_b are the reflectivities of the top and bottom DBR mirrors respectively, Γ is the confinement factor, L is the cavity length, and α_i is the internal loss of the cavity. The components of α_i are given as

$$\alpha_i = \Gamma\alpha_a + (1 - \Gamma)\alpha_b + \alpha_{sc} \tag{21}$$

where α_a is the loss per unit length in the active region, α_b is the loss per unit length in the passive region, and α_{sc} is the scattering loss for the cavity. The absorption loss for the $In_xGa_{1-x}As$ material in the QW region is typically about 30 cm^{-1}, the loss in the (Al,Ga)As barrier is about 10 cm^{-1} and the scattering loss is typically 20 cm^{-1}. If we define the
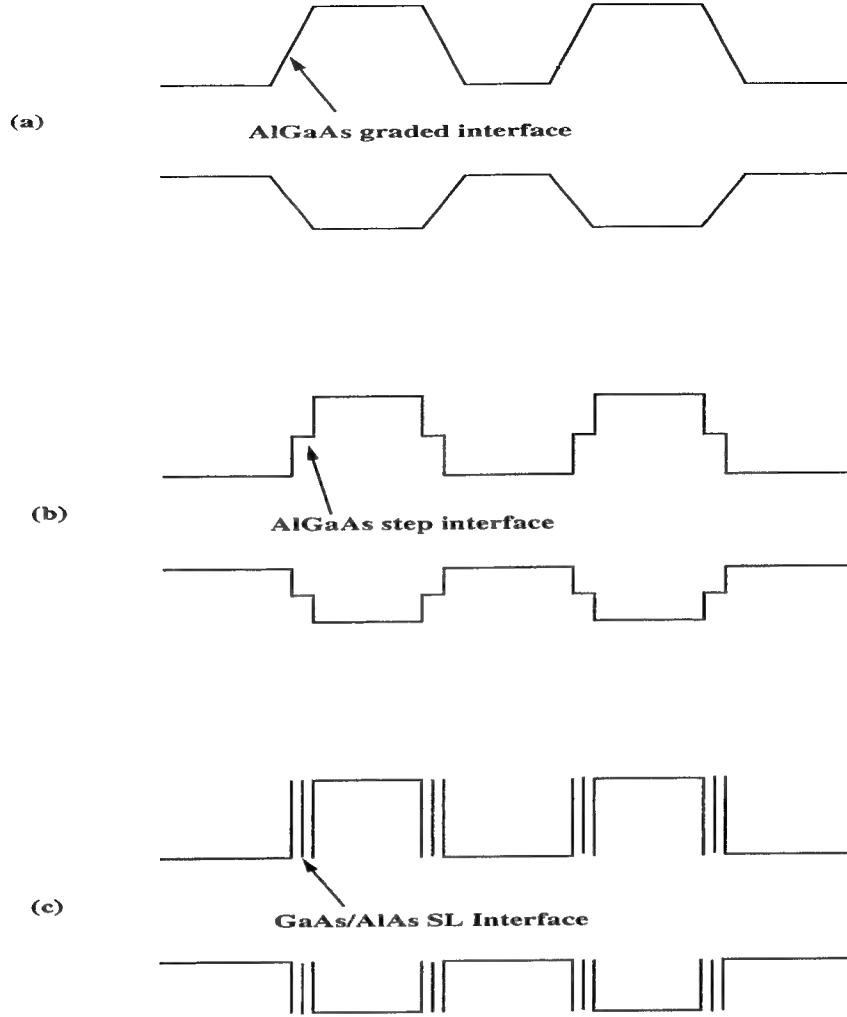
Fig. 3.2 The energy band diagram of GaAs/AlAs quarter wave DBR mirror with (a) a graded $Al_xGa_{1-x}As$ interface, (b) an $Al_xGa_{1-x}As$ step-layer, and (c) a GaAs/AlAs superlattice in-between the GaAs and AlAs layers.

confinement factor of the cavity as

$$\Gamma = \frac{\int_{active} E^2(z)\, dz}{\int_L E^2(z)}\, dz, \qquad (22)$$

one can compute this parameter. As an example, let us consider the electric field distribution

in the cavity as a standing waveform described by

$$E(z) = E_0 \cos(kz) \qquad (23)$$

with $k = 2\pi/\lambda$. Substituting this into Eqn. (22), one can find the expression for the confinement factor.
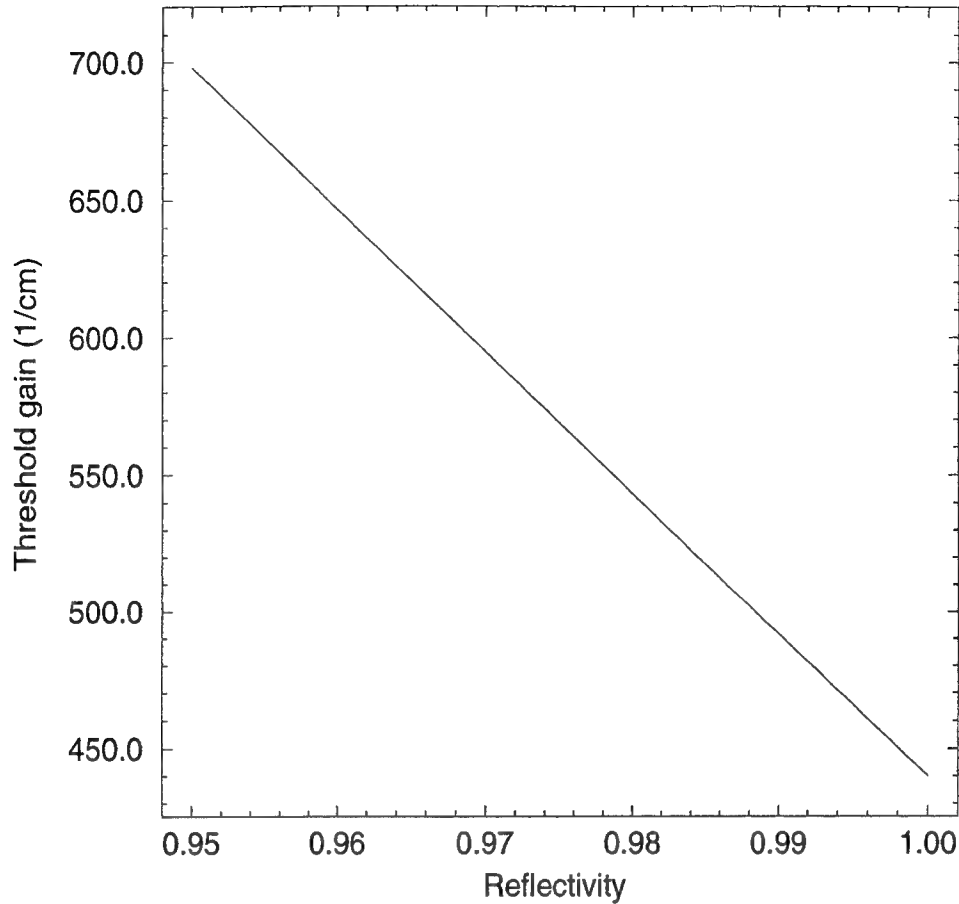
Fig. 4.1: The calculated threshold gain as a function of the mean reflectivity of a DBR mirror.

The threshold gain as a function of the mean reflectivity R for a VCSEL with a single (In,Ga)As/GaAs QW in the active region has a rather revealing form. This gain, plotted as a function of the mean reflectivity R, is shown in Fig. 4.1 As is evident from this figure, the gain required to reach threshold decreases as the mean reflectivity increases; this is to be expected from purely qualitative reasoning.

We now consider the differential quantum efficiency of a VCSEL. Assuming that there is no free carrier absorption at the bottom DBR mirror, from which the light is emitted, the differential quantum efficiency, η_d, can be expressed as

$$\eta_d = \eta_i \frac{\ell n(1/R_b)}{2\alpha L + \ell n(1/R_t R_b)}. \tag{24}$$

The calculated result for a (In,Ga)As/GaAs QW VCSEL with an indium mole fraction of 20% is shown in Fig. 4.2; the reflectivity of the top DBR mirror, R_t, is assumed to be 100%. Again, as expected, the external quantum efficiency decreases as the reflectivity of the output mirror increases. One must therefore compromise between low threshold gain
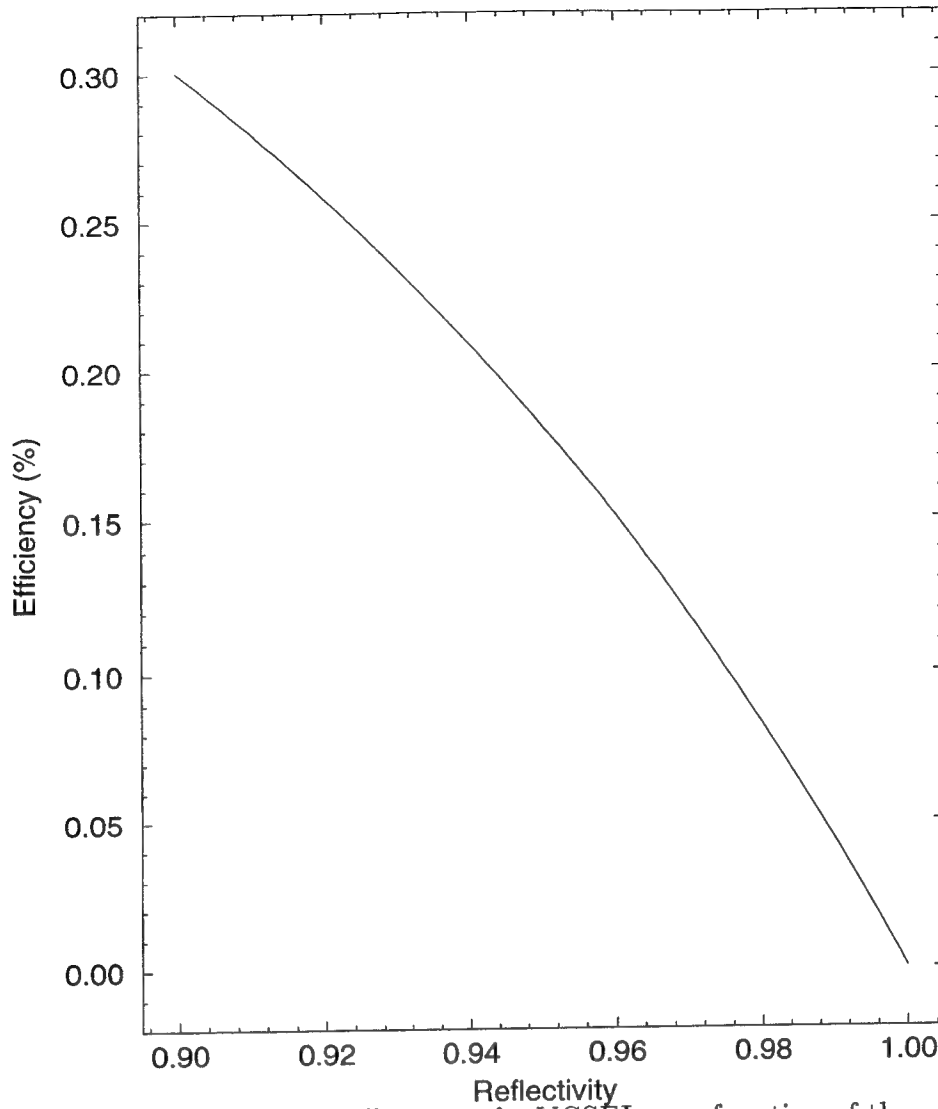
Fig. 4.2: The external quantum efficiency of a VCSEL as a function of the mean reflectivity of the mirror.

and high external quantum efficiency. This is a trade-off which must be dealt with in the design optimization process.

Another important parameter for evaluating device performance is the ratio of the optical power output to the total input power; this is the so-called *wall-plug* efficiency. It is defined symbolically as

$$\eta = \frac{P_0}{VI} = \eta_i \left[\frac{I - I_t}{I} \right] \left[\frac{h\upsilon}{eV_A} \right] \left[\frac{\ell n(1/R)}{\alpha L + \ell n(1/R)} \right] \qquad (25)$$

where I_t is the transparency current and V_A is the voltage applied to the device. For edge-emitting laser devices, values of $\eta \sim 30\%$ have been achieved at 300 K. For VCSELs, the best value is around 17%, which is comparatively low due to the high series resistance of the device at the DBR mirrors.

20

5. Molecular Beam Epitaxy of III-V Compounds

The method of molecular beam epitaxy (MBE) emerged in early 1970's as a vital growth technique for semiconductor materials. It is an epitaxial growth process involving the reaction of one or more thermal beams of atoms or molecules with a crystalline surface under ultrahigh vacuum conditions. The system in our laboratory consists of three vacuum chambers: one loading chamber, one transfer chamber and one growth chamber. These chambers are separated by isolation valves. The growth chamber is kept at an extremely ultrahigh vacuum condition. Using liquid nitrogen cryo-shrouding, the pressure of the growth chamber can be made to be below 10^{-10} Torr. There are several Knudsen cells mounted in the cell flange containing group III and V elements. Molecular or atomic beams are generated thermally from the Knudsen cells where quasi-equilibrium is maintained. The beam intensity from each cell is controlled by the cell temperature. These fluxes are guided and controlled by orifices and shutters and travel in straight paths to the substrate. For each cell, there is an individual shutter and then in front of all the shutters is a main shutter interposed between the substrate holder and the cells. In our system, the individual shutters are operated by high-speed motors and the main shutter is manually operated. The growth chamber is equipped with a flux gauge to measure the fluxes from the Knudsen cells for growth rate estimation. A residual gas analyzer with a sensor head mounted inside the growth chamber is used to monitor the residual gas species and system purity level. In our system, a reflection high energy diffraction (RHEED) is used for in-situ monitoring of the growth process. The RHEED is vital for monitoring the surface condition of the substrate, the growth dynamics and especially for determining the growth rate of the layers being grown. Our system is also equipped with an infrared pyrometer facing the substrate holder through a view to monitor the surface temperature of the substrate during the growth.

Since the growth of III-V compounds, such as GaAs, is a process of absorption and desorption of atoms from the substrate surface, the substrate temperature and V/III flux ratio are two of the important factors which affect material quality. For high quality optical materials, growth temperatures higher than 600°C are needed. It has been determined by many researchers that GaAs layers grown at higher substrate temperatures have higher luminescence efficiency because fewer impurity atoms are incorporated during the growth and furthermore, fewer defects are incorporated. It is now known that the V/III flux ratio during epitaxy greatly influences the incorporation of some dopants (Si,Be) and also of

some impurities which ultimately affect the material quality. The optimum V/III ratio is that which maintains an As_4-stabilized surface; this condition strongly depends on the substrate temperature. Low As_4 flux will generally lead to Ga-rich conditions which cause non-stoichiometric growth and may eventually result in loss of epitaxy and a rough surface morphology. An excess of As_4 flux, on the other hand, leads to high concentrations of deep levels, which lower the luminescence efficiencies of the material. It is important, therefore, that the substrate temperature and V/III flux ratio be optimized simultaneously. This is generally done through a combination of *ex-situ* characterization techniques.

5.1. Growth Rate Determination by RHEED

The precise determination of the growth rate of GaAs and the other related alloys is generally a challenge for the MBE community. For most approximate measurements, a thick layer—about a few microns—of the material of interest is grown. The thickness of this layer is then measured by a scanning electron microscope (SEM) after the growth. By knowing the total growth time and the thickness, one can then calculate the growth rate for use in future growths. For the precise layer thickness required for VCSEL structures—only errors of less than a few per cent are tolerated—the SEM thickness determination is not adequate. The RHEED oscillation technique has emerged as the only viable method for the stringent thickness requirements of the VCSEL.

During epitaxy, the RHEED pattern of growing layer structures usually oscillate as the growth proceeds. The period of the oscillation corresponds exactly to the growth of a single monolayer. So by determining the period of oscillation during growth, one can accurately measure the growth rate. The necessary condition to get strong RHEED oscillations is to commence the growth on a smooth substrate. Usually, after 30 seconds or so of initial growth, the oscillations die out because the surface becomes rough again. To measure the intensity of the RHEED oscillations, we use a fiber-optic light guide coupled to a detector system to collect the optical signal from the diffraction pattern on the phosphor screen. The detector signal is amplified before it is fed to an A/D converter. The digitized data is stored in a computer and can be manipulated. The oscillation frequency of the RHEED signal is determined by processing the stored data using a Fourier transform program.

Typically, to determine the growth rate of a GaAs or an (Al,Ga)As layer on a GaAs sub-

strate, a small, clean piece of GaAs wafer—about 1 cm × 1 cm—mounted on a molybdenum block. Our experience shows that a small size substrate gives the best oscillation signal from which an accurate growth rate can be determined. This is because it is easier to locate the electron beam from the RHEED gun onto the center of the small wafer and hence eliminate errors caused by rate variations across a large wafer. The RHEED oscillation measurement procedure is as follows. After the substrate has been heated to about 580°C, under Arsenic flux, the native oxide is desorbed and a sharp RHEED pattern is observed. Simultaneously, the pyrometer is calibrated for substrate temperature measurement later on. After about 40 seconds or so, the substrate temperature is raised to 610°C and the Ga cell shutter is opened to allow the growth of 1000 Å of GaAs. The growth is interrupted by closing the Ga cell shutter and the substrate temperature is simultaneously lowered to 580°. The re-evaporation of GaAs is negligible at this temperature. The RHEED oscillation frequency measurement is then conducted by opening either Ga for GaAs or both Ga and Al cell shutters for (Al,Ga)As

Because a Knudsen cell is typically at thermal equilibrium when the cell shutter is closed, the flux effusing from it right after the shutter is open is not at equilibrium. Flux transient effects are observed right after opening the shutter; the flux typically decays exponentially to a stable value in a 2 minute interval. It is, therefore, incorrect to measure the RHEED oscillations immediately after an individual shutter—such as that of Ga—has been opened. The values measured are transient and not steady-state. To avoid this transient effect, the main shutter is kept closed during the opening of the individual cell shutter for at least 2 minutes to allow the flux to stabilize; when the main shutter is opened after the flux has stabilized, the RHEED oscillation data can then be taken. This, in our opinion, is the best way to accurately determine the growth rates for GaAs, AlAs or (Al,Ga)As. The RHEED oscillation data for GaAs at the stabilized flux condition for $T_{Ga} = 940°C$ is shown in Fig. 4.3. By Fourier transform methods, we find that the frequency of oscillation is $f = 1.05$ Hz; the growth rate of the GaAs layer is therefore

$$\Gamma_{GaAs} = f\frac{a_0}{2} = f\frac{5.653}{2} = 2.973 Å \ / \ second. \tag{26}$$

As another example, we show in Fig. 4.4 the RHEED oscillation data for AlAs for an Al cell temperature of $T_{Al} = 1140°$. The AlAs growth rate determined from this curve is $\Gamma_{AlAs} = 2.2$ Å per second. When both Ga and Al cell shutters are open, the RHEED oscillation curve for the resulting (Al,Ga)As layer is shown in Fig. 4.5. The growth rate for the (Al,Ga)As layer is $\Gamma_{AlGaAs} = 4.9$ Å per second. From the growth rate data for these growths, we find

that

$$\Gamma_{AlGaAs} = \Gamma_{GaAs} + \Gamma_{AlAs} \qquad (27)$$

Knowing the growth rates for the GaAs and the (Al,Ga)As layers, one can determine the AlAs mole fraction from the x in $Al_x Ga_{1-x} As$ alloy. This fraction x is given as

$$x = \frac{\Gamma_{AlGaAs} - \Gamma_{GaAs}}{\Gamma_{AlGaAs}} \qquad (28)$$

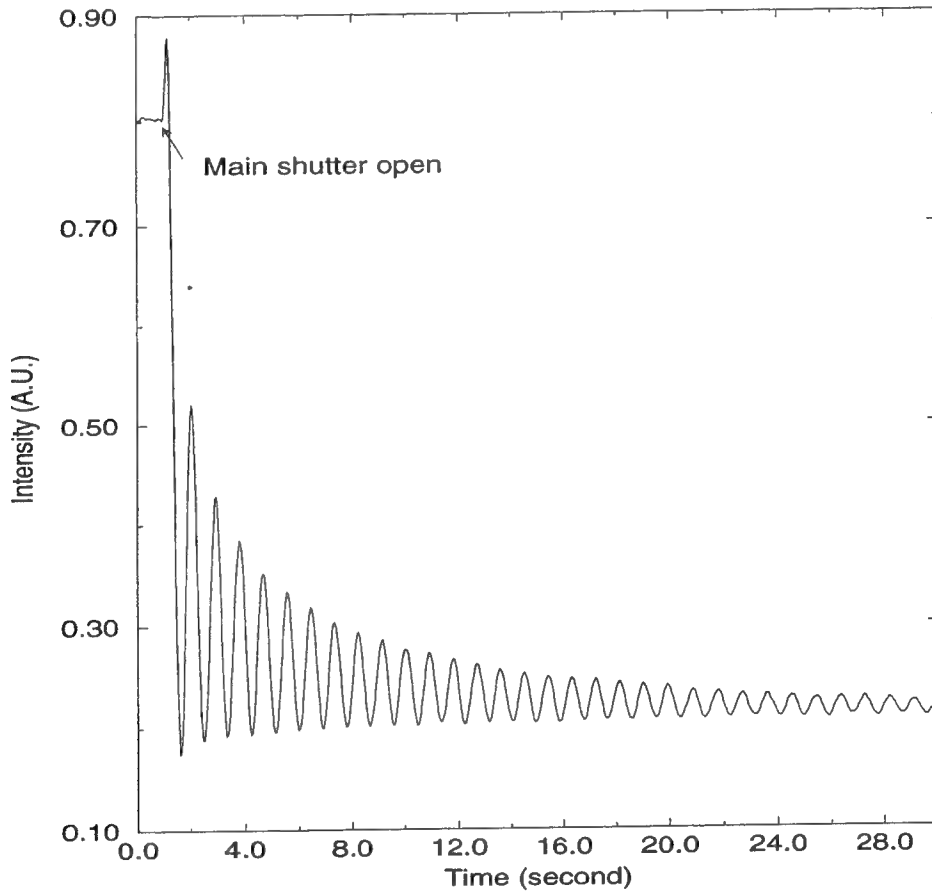This empirical equation is also valid for the other ternary alloys such as $In_x Ga_{1-x} As$.

Fig. 4.3. RHEED oscillations of a GaAs surface on a (001) GaAs substrate at a substrate temperature of 580°.
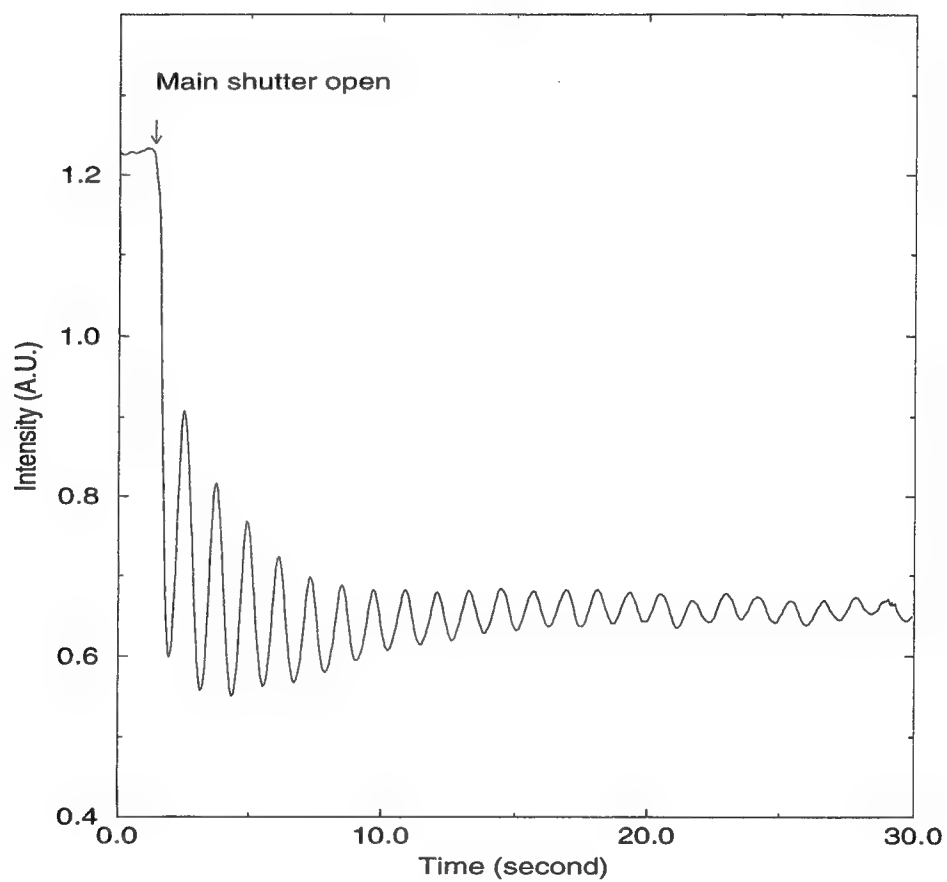
Fig. 4.4. RHEED oscillations of an AlAs surface on a (001) GaAs substrate at a substrate temperature at 580°.
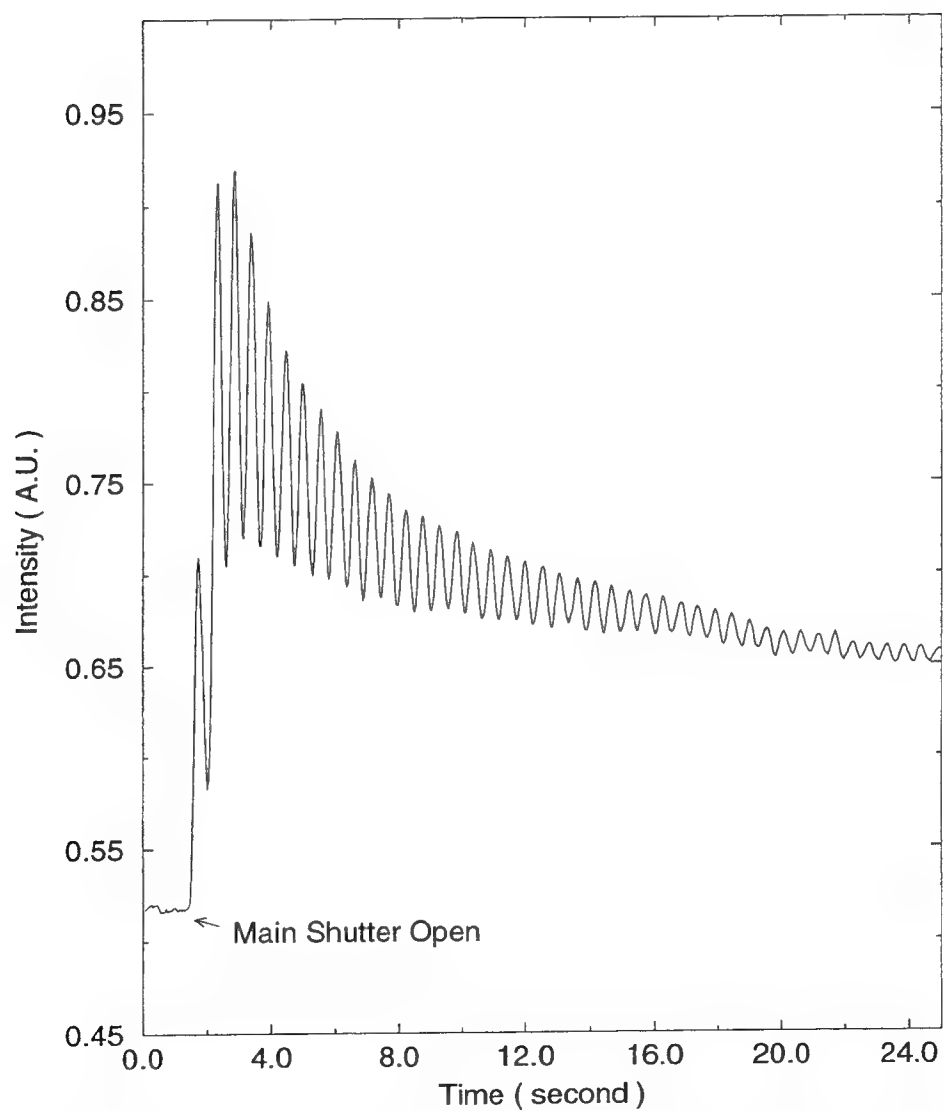
Fig. 4.5. RHEED oscillations of a (Al,Ga)As surface on a (001) GaAs substrate at a substrate temperature at 580°.

6. Polarization of Vertical-Cavity Surface-Emitting Lasers

In some applications, such as magneto-optic recording and coherent signal processing, the stability and the predictability of the polarization state of a vertical-cavity surface-emitting laser is very important. In most VCSELs grown on the (001) crystal surface of GaAs, there is no intrinsic mechanism for setting the laser polarization and, as a consequence, most reported polarization states of these devices are random. In a conventional edge-emitting laser, the relatively large loss experienced by the transverse magnetic (TM) modes of oscillation favors the transverse electric (TE) modes which have low loss. As a result, most light emitted by edge-emitting lasers is predominantly TE-polarized, and predictable. The isotropic in-plane gain distribution in VCSEL devices is mainly responsible for the lack of polarization stability [7,8]. Several techniques to impose polarization control have been investigated by several groups [9-11]. Some of these methods were discussed in the introduction and will not be repeated here.

In this section we illustrate the difficulty of obtaining polarization control in VCSEL devices grown on (001) GaAs substrates. In a subsequent section, we then offer our own approach to solving the polarization stability of VCSEL devices.

The polarization characteristics studied here are of index-guided, square VCSELs fabricated on monolithic structures grown on (001) substrates by wet-chemical etching techniques. We find that the orthogonal eigen-polarizations of these VCSELs are affected by the asymmetric transverse geometric shapes introduced during wet-chemical etching.

All the device structures studied here were grown by the technique of molecular beam epitaxy as described in a preceding section. The active region and the composite DBR mirrors were also designed and modeled as previously described. The structures consisted of 24 pairs of Si-doped ($n=2\times 10^{18}/cm^3$) quarter wave GaAs/AlAs stacks for the bottom DBR mirror, three $In_{0.18}Ga_{0.82}As$ (80 Å)/GaAs (80 Å) quantum wells in the center of a full-wave GaAs/$Al_{0.45}Ga_{0.55}As$ spacer region, and 19 pairs of Be-doped ($p=5\times10^{18}/cm^3$) quarter wave GaAs/AlAs stacks for the top DBR mirror; finally, a highly doped ($p=1\times10^{19}/cm^3$) GaAs layer for phase-matching to the gold contact metal was used as a cap. In order to reduce the series resistance, we have used a 100 Å thick $Al_{0.45}Ga_{0.55}As$ intermediate layer between the GaAs and AlAs quarter wave stacks. The DBR mirror structures were grown at 580°C and the $In_{0.18}Ga_{0.82}As$/GaAs quantum wells were grown at 520°C.

After growth, gain-guided devices with 50 μm square mesas were patterned using standard lithographic techniques. Two sets of devices were fabricated: in one set, the sides of the square mesa were aligned parallel to the <110> crystallographic axes as shown in the inset of Fig. 6.1; in the second set of devices, the sides of the mesa were aligned at 45° to the <110> crystallographic axes as shown in the inset of Fig. 6.2. The finished devices were tested under pulsed mode at room temperature. The pulse width was 0.4 μs with a 10 kHz repetition rate. The output light was measured using a calibrated Si detector. A linear polarizer was used to determine the polarization states of the devices.
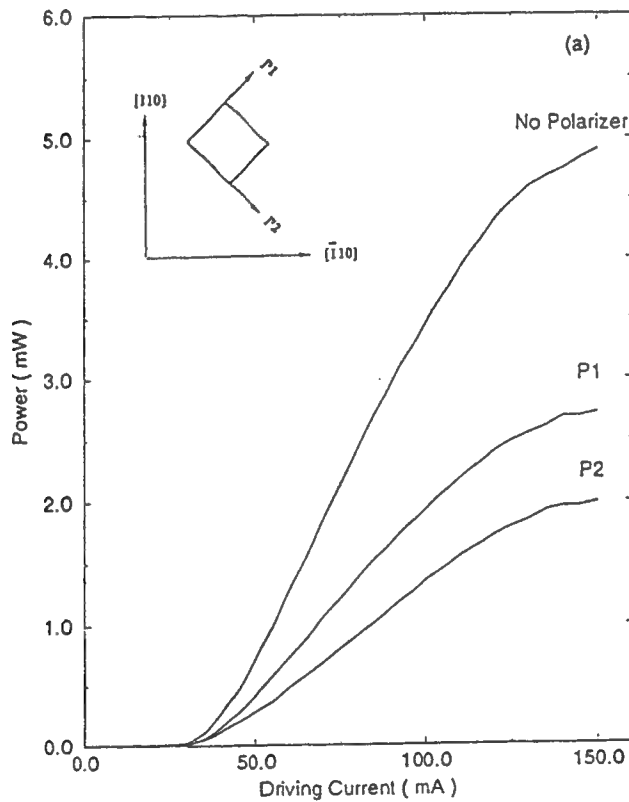

Fig. 6.1: Light output from a 50 μm square VCSEL with and without a polarizer aligned along the directions as shown in the inset.

For the first set of devices, two orthogonal polarization modes were detected for each device.

28

The light output for each of these polarizations as a function of driving current is shown in Fig. 6.1. It was found that the polarization state labeled **P1** was aligned along the [110] crystallographic axis and the polarization state labeled **P2** was aligned along the [$\bar{1}$10] crystallographic axis. The mode **P1** had a threshold current of 35 mA and the mode **P2** had a higher threshold current of 50 mA. The output power ratio for these two polarization modes at $3I_{th}$ was about 2.2. When similar polarization measurements were carried out for the devices in the second set, it was found that some devices had two modes of orthogonal polarizations aligned along the sides of the square mesa. Other devices, however, exhibited two orthogonal polarizations which were randomly aligned. These orthogonal polarizations had the same threshold current as the one measured for the first set of devices. The light output as a function of current for a typical device from the second set with the two polarizations parallel to the sides of the square is shown in Fig. 6.2.

These experiments provided simple demonstrations that there is no intrinsic mechanism for the control of the polarization state for VCSEL devices grown on the (001) GaAs surface. An artificial scheme for setting the polarization by fabrication-induced anisotropy may sometimes work, as demonstrated here. This method, however, is not reliable.

In the next section, we briefly discuss an alternative approach to achieving a measure of control on the polarization eigenstates of vertical-cavity surface-emitting lasers.
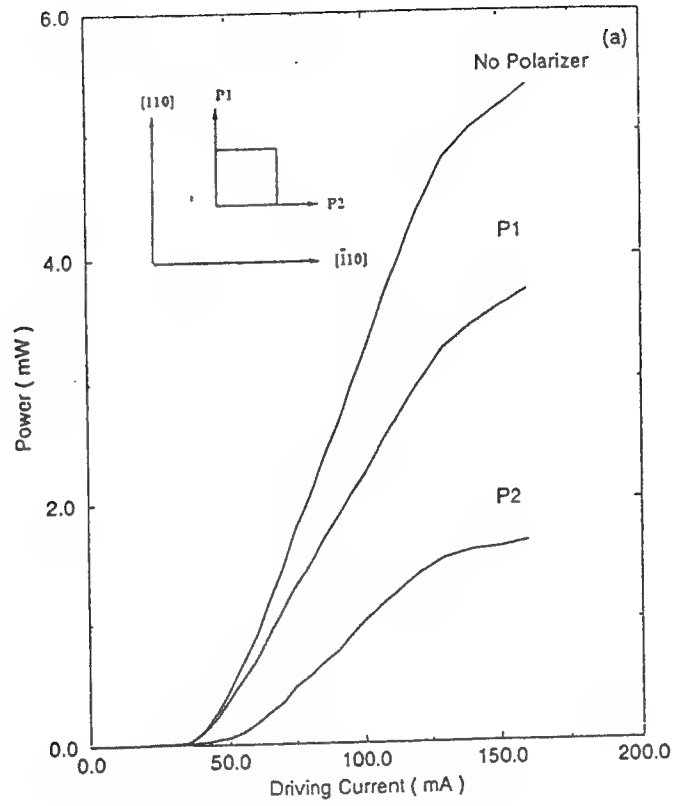
Fig. 6.2: Light output from a 50 μm square VCSEL with and without a polarizer aligned along the directions as shown in the inset.

7.   Stable Polarization Characteristics of Vertical-Cavity Surface-Emitting Lasers on (110) GaAs Substrates

As discussed earlier, most VCSEL structures have been grown on GaAs substrates oriented in the conventional [001] crystal direction. We have recently found that quantum well structures grown on (110) GaAs substrates have anisotropic optical properties [22]; in an effort to explore the use of this anisotropy in the control of the polarization characteristics of VCSELs, we have fabricated devices grown on (110) GaAs substrates. Our room temperature optical pumping experiments show that the [110]-oriented VCSEL structures have stable polarization characteristics.

The VCSEL structures used in this particular study consist of a bottom DBR made of a stack of 19.5 GaAs/AlAs quarter wave pairs. The active region consists of two $In_{0.20}Ga_{0.80}As$ (80 Å)/GaAs (80 Å) quantum wells in the middle of a one-wave GaAs/$Al_{0.45}Ga_{0.55}As$ spacer region. The top DBR mirror is composed of a stack of 16 GaAs/AlAs quarter wave pairs. These structures were on semi-insulating (110) GaAs substrates which were vicinally mis-oriented by 6° toward (111)B surface in order to obtain high quality optical material [23]. For purposes of comparison, identical device structures were also grown on the (001) GaAs surface.

We show in Fig. 7.1, the reflectivity spectrum of the VCSEL structure grown on the (110) GaAs surface; shown in Fig. 7.2 is the lasing spectrum of the device. The optical pumping experiments were carried out at room temperature using a tunable laser source which could be operated in both the pulsed and continuous mode. The state of polarization of the laser was analyzed using a prism polarizer. The output of the device exhibited two orthogonal polarization states: the polarization state with maximum optical intensity was oriented along the [$\bar{1}$10] direction. Several spots were tested on the wafer; all of these spots showed similar polarization characteristics. The output intensity as a function of optical pumping power for the two orthogonal polarization states is displayed in Fig. 7.3. The intensity contrast ratio of the two orthogonal states of polarization for a pumping power of 70 mW incident onto a 10 μm-diameter spot size is about 4. In contrast, the optically-pumped VCSEL devices grown on the (001) GaAs substrate exhibited random polarization directions from spot to spot. We observed no preference of polarization direction for the (001) devices.
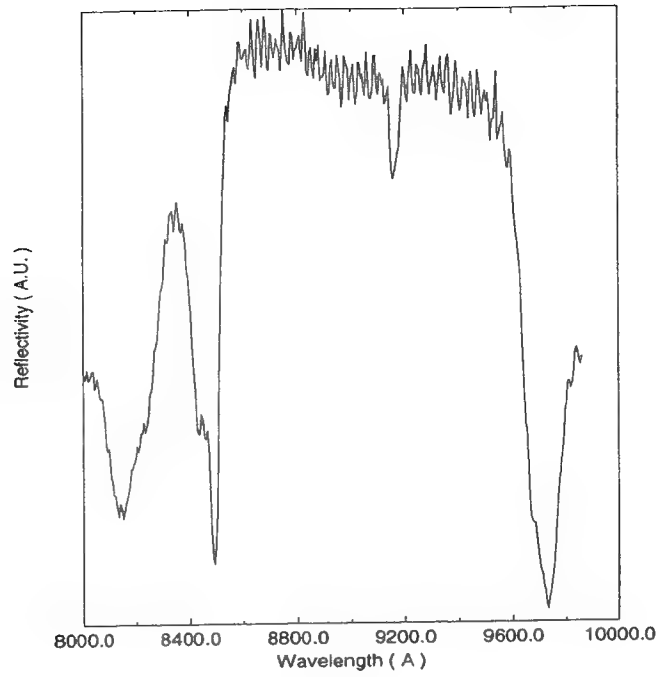
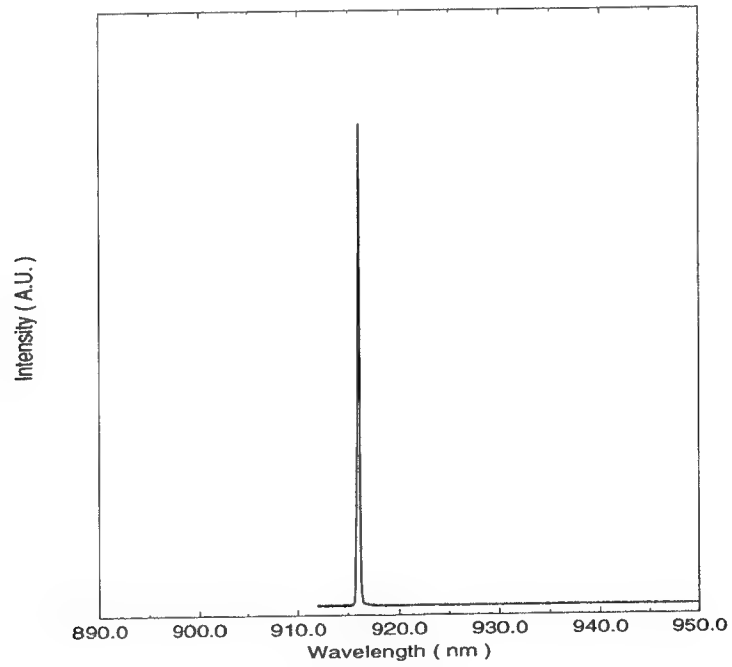Fig. 7.1: The reflectivity spectrum of a VCSEL grown on a (110) GaAs substrate

Fig. 7.2: The lasing spectrum of a VCSEL grown on a (110) GaAs substrate

In essence, these experiments demonstrate that the polarization characteristics of VC-SEL devices grown on (110) substrates are stable and have definite directional properties. Devices on the conventional (001) substrates exhibit a randomness to the directionality of the the polarization.
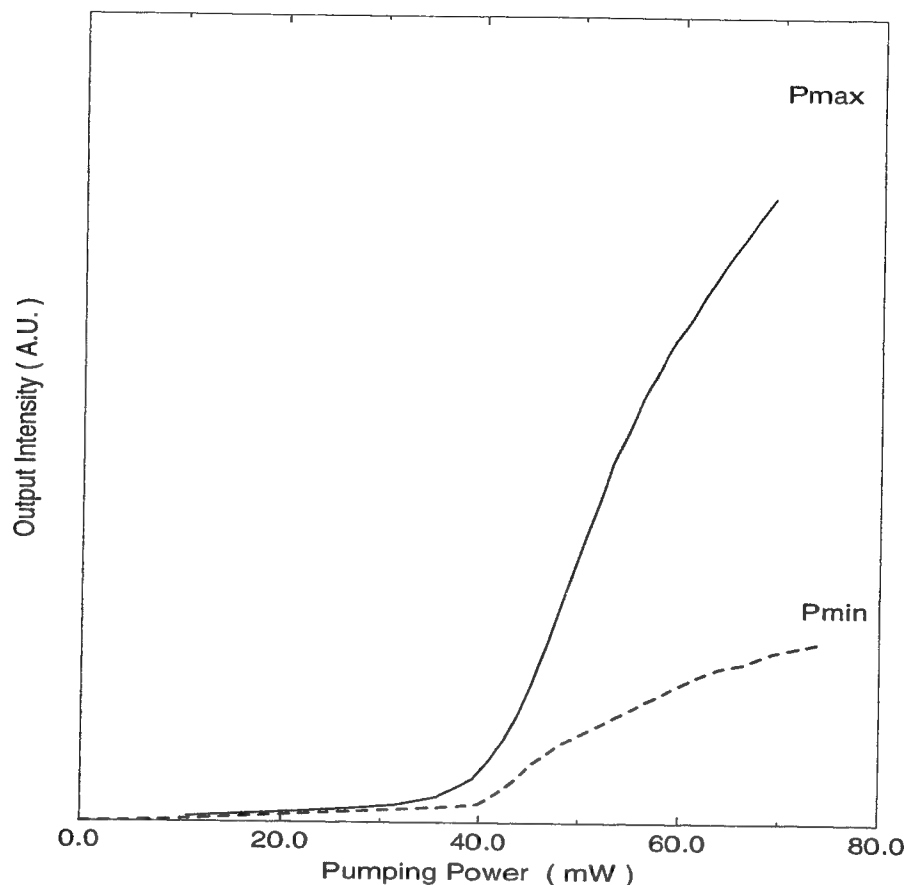

Fig. 7.3: The light output of a VCSEL grown on a (110) GaAs substrate as a function of optical pump power for the two stable eigen polarizations.

8. Summary

This document reported on the approach taken in designing practical vertical-cavity surface-emitting lasers. The device designs were implemented on structures grown by molecular beam epitaxy. Initially, conventional VCSEL devices grown on (001) GaAs substrates with an emission wavelength at 980 nm were fabricated. These devices were satisfactorily tested and characterized. Advanced research into the control of the polarization eigenstates of the

VCSEL devices was also initiated. Preliminary results of the advanced research show that devices fabricated on the unconventional (110) GaAs substrate exhibit stable polarization eigenstates.

In the next contract period, the goals of this research will be to design packages so that packaged devices can be manufactured and characterized. With appropriate packaging, it is anticipated that matrix-addressable devices will also be made. It is hoped that the packaged devices can be used in experiments at either Rome Laboratory or at the Air Force Institute of Technology.

References

[1] K. Iga, F. Yoyama, and S. Kinoshita, "Surface-emitting semiconductor lasers", IEEE J. Quantum Electron., **24**, 1845 (1988).

[2] J. L. Jewell, J. P. Harbison, A. Scherer, Y. H. Lee, and L. T. Florez, "Vertical cavity surface emitting lasers: design, growth, fabrication, characterization", IEEE J. Quantum Electron., **27**, 1332 (1991).

[3] C. J. Chang-Hasnain, J. P. Harbison, C. E. Zah, M. W. Maeda, L. T. Florez, N. G. Stoffel, and T. P. Lee, "Multiple wavelength tunable surface-emitting laser arrays", IEEE J. Quantum Electron., **27**, 1368 (1991).

[4] A. V. Lehmen, C. Chang-Hasnain, J. Wullert, L. Carrison, N. Stoffel, L. Florez, J. Harbison, "Independently addressable InGaAs/GaAs vertical cavity surface emitting laser arrays", Electron. Lett., **27**, 583 (1991).

[5] R. S. Geels, and L. A. Coldren, "Submilliamp threshold vertical cavity surface emitting laser diodes", Appl. Phys. Lett., **57**, 1605 (1990).

[6] R. S. Geels and L. A. Coldren, "Submilliampere Threshold Vertical-Cavity Surface-Emitting Laser Diodes," Appl. Phys. Lett., **57** 1605 (1990).

[7] T. Wipiejewski, K. Panzlaff, E. Zeed, and K. J. Ebeling, "Tunanle extremely low threshold vertical cavity surface emitting laser diodes", IEEE Photonics Tech. Lett., **5**, 889 (1993).

[8] R. P. Schneider, Jr. R. P. Bryan, J. A. Lott. G. R. Olbright, "Visible (657 nm) In-GaP/InAlGaP strained quantum well laser", Appl. Phys. Lett., **60**, 1830 (1992).

[9] C. J. Chang-Hasnain, J. P. Harbison, L. T. Florez, N. G. Stoffel, "Polarization characteristics of quantum well vertical cavity surface emitting lasers", Electron. Lett., **27**, 163 (1991).

[10] D. Sun and E. Towe, "Polarization characteristics of index-guided InGaAs quantum well vertical cavity surface emitting lasers", Unpublished.

[11] M. Shimizu, T. Mukaihara, T. Baba, F. Koyama, and K. Iga, "A method of polarization stabilization in surface emitting lasers", Jpn. J. Appl. Phys., **30**, l1015 (1991).

[12] T. Mukaihara, F. Koyama, and K. Iga, "Polarization control of surface emitting lasers by anisotropic biaxial strain", Jpn. J. Appl. Phys., **31**, 1389 (1992).

[13] K. D. Choquette, K. L. Lear, R. E. Leibenguth, and M. T. Asom, "Vertical cavity laser diode polarization switching and control", The Abstracts of 51st Annual Device Research Conference, June 21-23, 1993, University of California, Santa Barbara, CA.

[14] A. Chavez-Pirson, H. Ando, H. Saito, and H. Kanbe, "Polarization properties of a vertical cavity surface emitting laser using a fractional layer superlattice gain medium", Appl. Phys. Lett., **62**, 3082 (1993).

[15] E. Yablonovitch, E. O. Kane, "Band structure engineering of semiconductor lasers for optical communications", J. Lightwave Tech. **6**, 1292 (1988).

[16] J. M. Luttinger, "Quantum theory of cyclotron resonance in semiconductors: general theory", Phys. Rev. **102**, 1030 (1956).

[17] M. Born and E. Wolf, Principles of Optics, Pergamon Press, 1959.

[18] M. A. Afromowitz, "Refractive index of $Ga_xAl_{1-x}As$", Solid State Commun., **15**, 56 (1974).

[19] R. S. Geels, S. W. Corzine, and L. A. Coldren, "InGaAs vertical cavity surface emitting lasers", IEEE J. Quantum Electron., **27**, 1359 (1991).

[20] K. Tai, L. Yang, Y. H. Wang, J. D. Wynn, and A. Y. Cho, "Drastic reduction of series resistance in doped semiconductor distributed Bragg reflectors for surface-emitting lasers", Appl. Phys. Lett., **56**, 2496 (1990).

[21] E. F. Schubert, L. W. Tu, G. J. Zydzik, R. F. Kopf, A. Bervennti, and M. R. Pinto, "Elimination of heterojunction band discontinuity by modulation doping", Appl. Phys. Lett., **60**, 466 (1992).

[22] D. Sun, E. Towe, M. Hayduk and R. Boncek,"Observation of polarization-dependent electroabsorption in (In,Ga)As/GaAs modulator structures oriented in the [110] crystallographic direction", Appl. Phys. Lett. **63**, 166 (1993).

[23] D. Sun and E. Towe, "Molecular beam epitaxial growth of (Al,Ga)As/GaAs heterostructures and Si doping characterization study on vicinal (110) GaAs substrates", J. Crystal Growth, **132**, 2882 (1993).

Rome Laboratory

Customer Satisfaction Survey

RL-TR-_____

Please complete this survey, and mail to RL/IMPS,
26 Electronic Pky, Griffiss AFB NY 13441-4514. Your assessment and
feedback regarding this technical report will allow Rome Laboratory
to have a vehicle to continuously improve our methods of research,
publication, and customer satisfaction. Your assistance is greatly
appreciated.
Thank You

_____
_____

Organization Name:_____(Optional)

Organization POC: _____(Optional)

Address:_____

1.   On a scale of 1 to 5 how would you rate the technology
developed under this research?

        5-Extremely Useful   1-Not Useful/Wasteful

                       Rating_____

Please use the space below to comment on your rating. Please
suggest improvements. Use the back of this sheet if necessary.

2.   Do any specific areas of the report stand out as exceptional?

                    Yes____ No_____

    If yes, please identify the area(s), and comment on what
aspects make them "stand out."

3. Do any specific areas of the report stand out as inferior?

Yes___ No___

If yes, please identify the area(s), and comment on what aspects make them "stand out."

4. Please utilize the space below to comment on any other aspects of the report. Comments on both technical content and reporting format are desired.

MISSION

OF

ROME LABORATORY

Mission. The mission of Rome Laboratory is to advance the science and technologies of command, control, communications and intelligence and to transition them into systems to meet customer needs. To achieve this, Rome Lab:

a. Conducts vigorous research, development and test programs in all applicable technologies;

b. Transitions technology to current and future systems to improve operational capability, readiness, and supportability;

c. Provides a full range of technical support to Air Force Materiel Command product centers and other Air Force organizations;

d. Promotes transfer of technology to the private sector;

e. Maintains leading edge technological expertise in the areas of surveillance, communications, command and control, intelligence, reliability science, electro-magnetic technology, photonics, signal processing, and computational science.

The thrust areas of technical competence include: Surveillance, Communications, Command and Control, Intelligence, Signal Processing, Computer Science and Technology, Electromagnetic Technology, Photonics and Reliability Sciences.